

Dynamics of Excess Electronic Charge in Aliphatic Ionic Liquids Containing the Bis(trifluoromethylsulfonyl)amide Anion

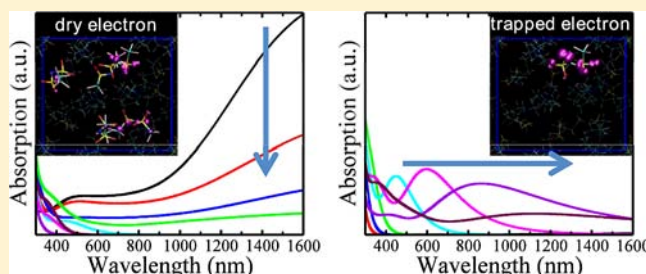
Changhui Xu,[†] Aleksander Durumeric,[†] Hemant K. Kashyap,[†] Jorge Kohanoff,[‡] and Claudio J. Margulis^{*†}

[†]Department of Chemistry, University of Iowa, Iowa City, Iowa 52241, United States

[‡]Atomistic Simulation Centre, Queen's University Belfast, BT7 1NN, United Kingdom

S Supporting Information

ABSTRACT: In a recent article (*J. Am. Chem. Soc.* **2011**, *133*, 20186) we investigated the initial spatial distribution of dry excess electrons in a series of room-temperature ionic liquids (RTILs). Perhaps unexpectedly, we found that in some alkylammonium-based systems the excess negative charge resided on anions and not on the positive cations. Following on these results, in the current paper we describe the time evolution of an excess electronic charge introduced in alkylammonium- and pyrrolidinium-based ionic liquids coupled with the bis(trifluoromethylsulfonyl)amide ([Tf₂N⁻]) anion. We find that on a 50 fs time scale an initially delocalized excess electron localizes on a single [Tf₂N⁻] anion which begins a fragmentation process. Low-energy transitions have a very different physical origin on the several femtoseconds time scale when compared to what occurs on the picosecond time scale. At time zero, these are intraband transitions of the excess electron. However after 40 fs when the excess electronic charge localizes on a single anion, these transitions disappear, and the spectrum is dominated by electron-transfer transitions between the fragments of the doubly charged breaking anion.



1. INTRODUCTION

Recently, room-temperature ionic liquids (RTILs) have been the focus of intense research for the purpose of better understanding phenomena such as electron transfer and transport relevant to energy storage.^{1–8} Equally important and very much related is research that is focused on their environmental and technological relevance for applications in spent nuclear fuel recycling.^{9–13} Excess electrons produced via photoexcitation or radiolysis react to form other chemically active species. The study of these species provides a window of opportunity to better understand bimolecular electron-transfer reactions, solvent relaxation dynamics, charge transport, and other transient behavior on media that is often structurally and dynamically heterogeneous.

Although many of these liquids are fairly new, much has been already done experimentally to elucidate the nature of radiolytic pathways^{13–24} and degradation products^{11,25–32} as well as the nature of the reactive species when electrons are produced instead by photodetachment.^{33–37} Perhaps, less well-understood is the identity of the species giving rise to femtosecond and early picosecond processes that initiate the cascade of possible reactions that are observed at longer times. Concepts such as the dry or presolvated electron, the trapped electron, and the solvated electron are ubiquitous in the literature but little is still known about the actual nature of these species.^{17,21,35,38} What is the chemical, quantum mechanical, and structural nature of the species that undergo initial relaxation (i.e., what does a presolvated electron look like in

a RTIL)?^{39–41} And what is it meant by the concept of a trapped or caged electron? What actual physical processes are responsible for the relaxation that gives rise to major changes in the excess charge transient spectrum as it goes from dry to trapped and as the trapped state relaxes? Providing a clear answer to these questions is very important from a technological perspective because insight into the stability of the ions is needed for an informed selection of RTILs for specific applications.¹⁷

We attempt to make contact with recent ultrafast femtosecond results from photodetachment in the 1-methyl-1-butylpyrrolidinium bis(trifluoromethylsulfonyl)amide ([Pyr_{1,4}][Tf₂N]) system recently published by the Blank group³⁵ and the picosecond resolution electron solvation dynamics radiolysis experiments by Wishart¹⁷ on the same system. We also attempt to make contact with the experiments by the group of Takahashi on the *N,N,N*-trimethyl-*N*-propylammonium bis(trifluoromethylsulfonyl)amide ([N₁₁₃][Tf₂N]) system.²² Both experimental^{17,18,35} and computational⁴¹ works describe two optical absorption bands; the lower energy one in the near-IR region is mainly due to the excess electrons, and the higher energy band has multiple contributions from excess electrons and holes. The reason why the band in the near-IR is unequivocally assigned to the excess electron species is intensity bleaching upon the addition of electron scavengers.^{16,18,24,35} In

Received: September 9, 2013

Published: October 24, 2013

this article we are most interested in the near-IR band assigned to the excess electron. Work on the contribution of holes to the higher energy band in the visible range as well as the fate of the excess electron in the presence of scavengers will be the subject of future publications.

Yang and co-workers²¹ were the first group to achieve a 15 ps time resolution in the radiolysis study of *N,N*-diethyl-*N*-methyl-*N*-(2-methoxy)ammonium bis(trifluoromethylsulfonyl) amide ([DEMMA][Tf₂N]) in 2008. This work together with a follow up article in 2009 by Kondoh and co-workers,²⁴ which studied the time-dependent radiolysis of a larger family of alkylammonium and pyrrolidinium [Tf₂N⁻] based RTILs, arrived at the conclusion that the lifetime of the excess electrons is on the order of hundreds of nanoseconds. The solvation time scale, at least in the case of [DEMMA][Tf₂N], was reported to be 26 ps.²¹ Further work³³ by Takahashi and the group of Wishart on photodetrapment of solvated electrons confirms that photo-generated electrons in the [N₁₁₁₃][Tf₂N] system also have a lifetime of ~250 ns.

Perhaps the most relevant time-resolved radiolysis work on the [Pyr_{1,4}][Tf₂N] is that recently published by Wishart in 2012 using the pulse-probe technique.¹⁷ The time resolution in this experiment was reported to be between 9 and 14 ps and allows for the clear observation of a blue shift in the near-IR excess electron band as the electron undergoes solvation. The authors concluded that the full equilibration of the excess electron occurs on the subnanosecond time scale and proposed the formation of a new species, the trapped electron, which initially appears on a time scale faster than 15 ps and is responsible for the decrease of the transient absorption (TA) signal at the 1400–1600 nm range. Wishart and co-workers¹⁷ proposed that the trapped electron is not “the driest form” of the excess electron which should absorb at even lower energies. Recent time- and angle-resolved two-photon photoemission experiments on ionic liquid ultrathin films at the electrode and vacuum interfaces appear to indicate that a trapped electron state forms on a time scale faster than 100 fs.⁴² In our previous work⁴¹ in which we studied the dry excess electron, a prominent band at very low energies was observed and assigned to intraband transitions of the excess electron that were translational in nature. By this we meant that a delocalized excess charge could be displaced to a different location and delocalized on a nearby group of ions by low excitation energies. In the same article⁴¹ we proposed that at time zero after the injection of an excess charge in an IL, the pattern of charge localization was not obviously related to the positive or negative nature of the species in solution or the aromatic or aliphatic nature of the cations but instead directly related to the relative alignment of cationic and anionic electronic energy states in solution. In the case of liquids comprising aliphatic cations coupled with the [Tf₂N⁻] anion we found that at time zero, the excess electron delocalized over several anions. Instead, liquids involving the imidazolium ring coupled with the chloride anion showed localization on the cations.

Very recent work by the group of Blank³⁵ successfully probed the femtosecond dynamics of excess electrons and holes generated by photodetachment in the [Pyr_{1,4}][Tf₂N] system. These experiments have a clear advantage over previous attempts at studying femtosecond photolysis in RTILs because samples were flowed. The Blank group showed that without flowing the sample much of what can be measured corresponds to prior laser pulse degradation products and not the excess electron and hole. For technical reasons, these experiments

were not able to cover the maximum of the excess electron band at around 1100 nm which is the main focus of our current paper. Their measurements were at higher energies below 1000 nm and captured the transient absorption dynamics on the higher energy side of the near-IR excess electron band as well as the higher energy band at around 600 nm that appears to have contributions both from hole and electron species. Their conclusion agrees with our original prediction of shifted bimodal bands for the electron and hole species.⁴¹ Blank and co-workers concluded that more than one species is responsible for the signal at higher energies and that the excess electron is mostly responsible for the low energy band. The time evolution from 0.6 to 600 ps of these two peaks is different; the high-energy band decreases in intensity with time and the low-energy band increases in intensity. The intensity increase in the TA at around 900 nm is consistent with the blue shift observed by Wishart and co-workers in their picosecond resolution radiolysis studies,¹⁷ but the shape of the photodetachment spectrum appears bimodal.

In the following sections we will attempt to explain the chemical origin of the species giving rise to the near-IR band. We will describe the nature of the so-called dry and trapped electrons. We will make predictions about major spectroscopic changes that should be observed when experiments become available on a time scale shorter than 40 fs. We will interpret the quantum mechanical and geometric origin of these spectroscopic changes in the condensed phase as the electron goes from the dry state to the trapped state. Finally, we will also provide insight on the fate of species on the picosecond time scale.

2. METHODS

In order to study the dynamics of an excess electron in [Pyr_{1,4}][Tf₂N] and [N₁₁₁₃][Tf₂N], we performed *ab initio* molecular dynamics simulations. For both systems initial configurations were generated by classical molecular dynamics with the GROMACS package using the Canongia–Lopes and Pádua force field parameters^{43,44} except that dihedrals for the alkyl chain part were taken from the improved OPLS-AA force field.⁴⁵ This combination of potentials parameters properly reproduces experimental structure.⁴⁶ Both systems comprised 8 ion pairs (304 atoms in the case of [N₁₁₁₃][Tf₂N] and 360 atoms in the case of [Pyr_{1,4}][Tf₂N]). Systems were initially equilibrated at 300 K and 1 bar in the NPT ensemble for at least 3 ns. Densities and radial distribution functions are comparable to those obtained for larger simulation boxes.

The final configurations from our classical molecular dynamics simulations were used as a starting point for our *ab initio* studies. *Ab initio* simulations were performed using the SIESTA program,^{47–49} in which norm-conserving pseudopotentials replace core electrons, and atom-centered numerical basis sets are used to represent the valence electrons. All our studies use the nonrelativistic Troullier–Martins pseudopotentials⁵⁰ and the Perdew, Burke, and Ernzerhof (PBE)⁵¹ flavor of the generalized gradient approximation (GGA). The pseudopotentials were generated using the ATOM program in the SIESTA package. We carefully tested the pseudopotentials for the proper representation of the various possible excitation states of each atomic element. The default double- ζ plus polarization basis set was used with an energy shift set to 25 meV. The mesh cutoff was set to 250 Ry which gives a real space grid resolution of about 0.1 Å. Periodic boundary conditions are automatically applied in SIESTA. The Brillouin zone sampling was only conducted on the Γ -point, which is reasonable for our large liquid systems. In all our *ab initio* molecular dynamics simulations the electronic temperature was set to 100 K to smear the Fermi–Dirac occupation function.

For both systems, the starting configurations derived from our classical molecular dynamics simulations were initially relaxed

quantum mechanically using the conjugate gradient algorithm until the maximum force was 0.04 eV/Å or less per atom. The goal of this step was simply to adjust bond lengths and angles in our properly equilibrated condensed phase liquid configurations to the *ab initio* potential energy surface. Both systems were then subject to an *ab initio* annealing step that brought the temperature back to 300 K in 2.5 ps. A final *ab initio* dynamics equilibration step of 0.5 ps was run in the NVT ensemble using the Nosé thermostat keeping the temperature at 300 K. In each case the final configuration was used as initial coordinates for our production runs with the excess electron.

For each system, a single point spin restricted calculation ($S = 1/2$) was performed in the presence of the excess electron, and the resulting density matrix was used as initial condition for a single point spin unrestricted calculation. The final density matrix was then used as initial guess for our spin unrestricted molecular dynamics simulations. Throughout our runs we did not observe any significant spin contamination.

Our two production runs (one for each ionic liquid) in the presence of the excess electron were in the NVE ensemble with a time step of 1 fs. The total simulation time for each of these runs was 5 ps. Data were analyzed every 100 fs to generate spin densities, HOMO/LUMO wave functions, and the optical spectrum. To further analyze the early dynamics associated with the dry electron state, during the first 100 fs the data were processed every 10 fs. To analyze the transient behavior of the excess charge, atomic charges were calculated using Mulliken population analysis as coded in SIESTA. The imaginary part of the dielectric function ϵ_2 was calculated based on first-order perturbation theory using SIESTA. This function was then convoluted as in our previous study⁴¹ with a Gaussian function of 1 eV fwhm. This broadening is somewhat arbitrary but reasonable based on estimations in water and other systems.^{52–54} The real part of dielectric function ϵ_1 was calculated using the Kramers–Kronig relationship.^{55,56} The real and imaginary parts of the dielectric function were used to calculate the absorption spectra using eq 1.

$$\alpha = \frac{2\omega}{c} \sqrt{\frac{\epsilon_1^2 + \epsilon_2^2 - \epsilon_1}{2}} \quad (1)$$

In eq 1, α is the absorption coefficient, c is the speed of light, ω is the frequency, and ϵ_1 and ϵ_2 are the real and imaginary parts of the dielectric function. It is well-known that GGA underestimates the energy band gap, and this has an effect on electronic transitions across the gap, shifting the excitation threshold of the neat liquid to lower frequencies. This can be corrected by shifting rigidly the empty states in the required amount (scissor). In this work we have not accounted for this fact, which requires a computationally very intensive step to determine the magnitude of the scissor shift. The qualitative features discussed in this paper should not be significantly affected by this approximation, although the absolute position of peaks and relative distance between them may change.

3. RESULTS

3.1. The Nature of the Dry Electron. The term dry electron is often used to denote the physical state of an excess charge created either by photodetachment or by radiolysis before any form of chemical or structural relaxation in the system. Clearly, because of the short lifetime of this species its physical nature often remains elusive. The dry electron will take different forms dependent on the condensed phase media in which it is generated. Furthermore electrons generated in radiolysis experiments are likely to be of a different nature to those generated by photodetachment experiments. In the first case the electron will travel far enough from the hole that radiative recombination is very unlikely. In the second case the electron is vertically excited due to negligible momentum transfer from the photon. Therefore, electron and hole can potentially remain close together forming an excitonic state, which can decay by radiative recombination.

In our studies, an excess electron is introduced in condensed phase systems pre-equilibrated in the absence of the extra charge. It then represents better the first scenario realized in radiolysis experiments. Figure 1 (left) and (right) shows that before the addition of an excess electron, $[\text{N}_{1113}][\text{Tf}_2\text{N}]$ and $[\text{Pyrr}_{1,4}][\text{Tf}_2\text{N}]$ are transparent beyond 300 nm.

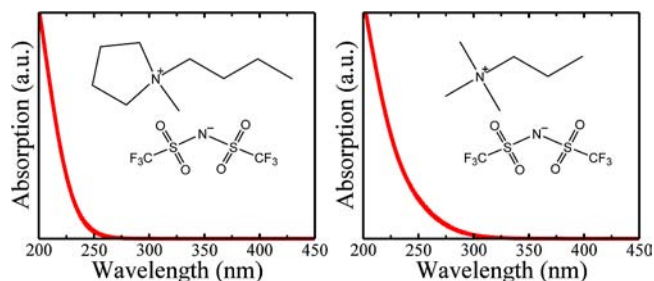


Figure 1. The optical absorption spectra for neat (left) $[\text{Pyrr}_{1,4}][\text{Tf}_2\text{N}]$, (right) $[\text{N}_{1113}][\text{Tf}_2\text{N}]$ showing that both liquids are transparent beyond about 300 nm. No signal is observed at larger values of λ .

Figure 2 shows the time evolution of the optical spectrum of the dry electron for the $[\text{N}_{1113}][\text{Tf}_2\text{N}]$ and the $[\text{Pyrr}_{1,4}][\text{Tf}_2\text{N}]$

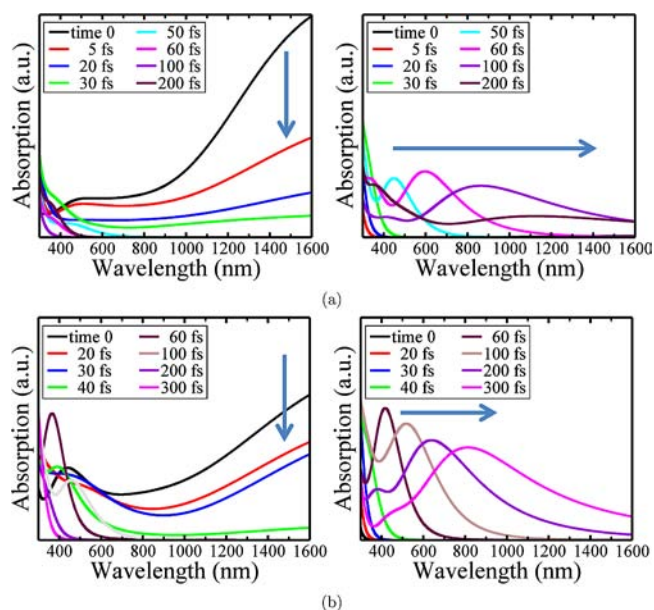


Figure 2. The early time-dependent optical absorption spectrum in the presence of an excess electron for (a) $[\text{Pyrr}_{1,4}][\text{Tf}_2\text{N}]$ and (b) $[\text{N}_{1113}][\text{Tf}_2\text{N}]$ ILs. In each case the left panel corresponds to the spin up channel (which includes the excess electron) and the right panel to the spin down channel. The spin up channel broad absorption band in the near-IR disappears on a 50 fs time scale, while a new band in the spin down channel appears at high energies and moves toward the red.

systems. In particular Figure 2a (left) and 2b (left) show the time-dependent spectrum of the spin up channel which contains the excess electron, whereas Figure 2a (right) and 2b (right) shows the spectrum of the spin down channel in the case of $[\text{Pyrr}_{1,4}][\text{Tf}_2\text{N}]$ and $[\text{N}_{1113}][\text{Tf}_2\text{N}]$, respectively.

Since the excess electron is in the spin up channel, at time zero, only transitions of this channel are possible for energies lower than about 3 eVs. This is because the spin down channel is comprised of electrons in valence bands of the neat liquid

which are several eVs below the excess electron singly occupied molecular orbital (SOMO) and LUMOs.^{41,57} A different way to put this is that the highest energy state of the spin down channel can be associated with the HOMO of the neat liquid in the absence of an excess charge. Since $[\text{Pyrr}_{1,4}][\text{Tf}_2\text{N}]$ and $[\text{N}_{1113}][\text{Tf}_2\text{N}]$ are transparent in the probed optical range, no transitions are expected from the spin down channel at time zero.

In what follows we will refer to the HOMO and LUMO states of neat liquids in the absence of the excess electrons as HOMO^0 and LUMO^0 , respectively. The SOMO and LUMO states of the spin up channel will be referred to as $\text{HOMO}\uparrow$, $\text{LUMO}\uparrow$, and the HOMO and LUMO states of the spin down channel as $\text{HOMO}\downarrow$, $\text{LUMO}\downarrow$ respectively.

Figure 2a (left) and 2b (left) shows that as time evolves on a femtosecond time scale the large band at very low energies in the near-IR corresponding to transitions from $\text{HOMO}\uparrow$ to a set of $\text{LUMO}\uparrow$ states quickly disappears until it is completely suppressed at about 50 fs. At the same time a new band at higher energies corresponding to the spin down channel emerges as is shown in Figure 2a (right) and 2b (right). Because of the completely different physical nature of these transitions the disappearance of the spin up channel near-IR band and the appearance of a visible band in the spin down channel define two different states of the electron. We assign the state that occurs between 0 and 50 fs with a very large absorption in the near-IR to the dry electron. The new band in the visible at 50 fs in the spin down channel reflects the appearance of the nascent trapped electron state. In the next subsection we will focus again on this band which will initially systematically red shift as the trapped electron state evolves.

A simple physical interpretation of the nature of the dry and trapped electrons in the $[\text{Pyrr}_{1,4}][\text{Tf}_2\text{N}]$ and $[\text{N}_{1113}][\text{Tf}_2\text{N}]$ systems can be derived from following the time dependence of the Mulliken charges of the ions. While this may not be the best possible scheme to determine accurate ionic charges, the Mulliken charge analysis gives a very clear picture of the early electronic localization events.⁵⁸ Figure 3 shows the time history of the ionic charge for each of our 16 periodically replicated ions in the case of $[\text{Pyrr}_{1,4}][\text{Tf}_2\text{N}]$ and $[\text{N}_{1113}][\text{Tf}_2\text{N}]$ (negative time corresponds to the neat liquids before introducing the excess charge). In our calculations 0.6–0.7 |e| is the typical absolute Mulliken charge of an individual ion. The noninteger values observed arise because Mulliken charges are not sufficiently accurate for partitioning charge when basis sets are nonorthogonal and nonminimal. They are, however, very useful to uncover trends as they vary in time. Figure 3 shows that at time zero and up to about 40 fs the excess charge is shared by three or more different anions. In both liquids, initial fast relaxation results in the localization of the charge on a single $[\text{Tf}_2\text{N}^-]$ anion which becomes doubly charged. This can be seen pictorially in Figure 4 where spin densities for both liquids are distributed initially across several anions but at later time “trap” on a single one. This is the physical origin of the very early trapped electron in these particular systems.

Yet another way to analyze the dry electron and its evolution toward the trapped state is by looking at the very early time history of the DFT energy eigenvalues. Figure 5a (left) and 5b (left) shows the initial time evolution of the energy eigenvalues in the spin up channel, whereas Figure 5a (right) and 5b (right) corresponds to the spin down channel in $[\text{Pyrr}_{1,4}][\text{Tf}_2\text{N}]$ and $[\text{N}_{1113}][\text{Tf}_2\text{N}]$, respectively. We remind the readers that in our calculations the excess electron is always in the spin up channel.

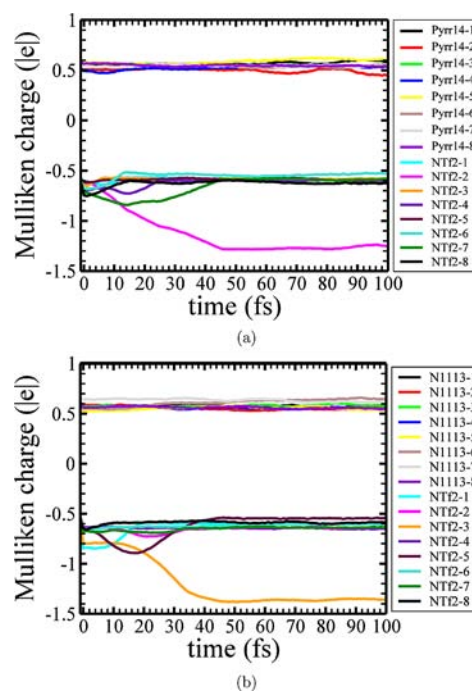


Figure 3. Early evolution of the Mulliken charges for all ions in the (a) $[\text{Pyrr}_{1,4}][\text{Tf}_2\text{N}]$ and (b) $[\text{N}_{1113}][\text{Tf}_2\text{N}]$ systems in the presence of an excess electron. After 40 fs the initially delocalized excess charge localizes on a single anion that undergoes significant structural changes. Negative time corresponds to the neat neutral systems before the addition of the excess charge.

In all of these figures HOMO and LUMO eigenvalues are denoted with blue and red dashes, respectively. For visual clarity HOMO states are connected with blue dotted lines, whereas LUMO states are connected with red dotted lines. In these graphs, at negative time we show also for reference the values of HOMO^0 (blue) and LUMO^0 (red). HOMO^0 corresponds to $\text{HOMO}\uparrow-1$ and LUMO^0 to $\text{HOMO}\uparrow$.

Figure 5a (left) and 5b (left) shows during the first 40 fs typical Stokes shift relaxation behavior after initial perturbation. By this we mean that $\text{HOMO}\uparrow$ and nearby $\text{LUMO}\uparrow$ states, which initially belong to the same band, move down in energy, whereas the fully occupied bulk liquid band several eVs below moves up in energy. Low-energy transitions between $\text{HOMO}\uparrow$ and $\text{LUMO}\uparrow$ states significantly contribute to the very broad band in the near-IR before 40 fs (see Figure 2 (left)). However, both $[\text{N}_{1113}][\text{Tf}_2\text{N}]$ and $[\text{Pyrr}_{1,4}][\text{Tf}_2\text{N}]$ undergo major changes in their electronic structure at about 40 fs. These changes break the symmetry of our liquids, and therefore $\text{HOMO}\uparrow$ and $\text{LUMO}\uparrow$ energies are no longer similar after 40 fs. By 40 fs $\text{HOMO}\uparrow$ localizes on a single anion which undergoes significant structural changes (see Figures S1 and S2). In both liquids, initial structural changes involve the elongation of one of the anionic S–N bonds followed by significant changes in the S–N–S angle at later time. This localization process can be followed in Figure 4 where we plot time-dependent spin densities for each of our systems. The nature of the symmetry that is broken after 40 fs is simple to rationalize. At this point the excess electron has found an energy trap, and different locations in the liquid are no longer energetically semi-equivalent. We remind the reader that initially, transitions between $\text{HOMO}\uparrow$ and several $\text{LUMO}\uparrow$ states corresponded to translations of the excess electron to

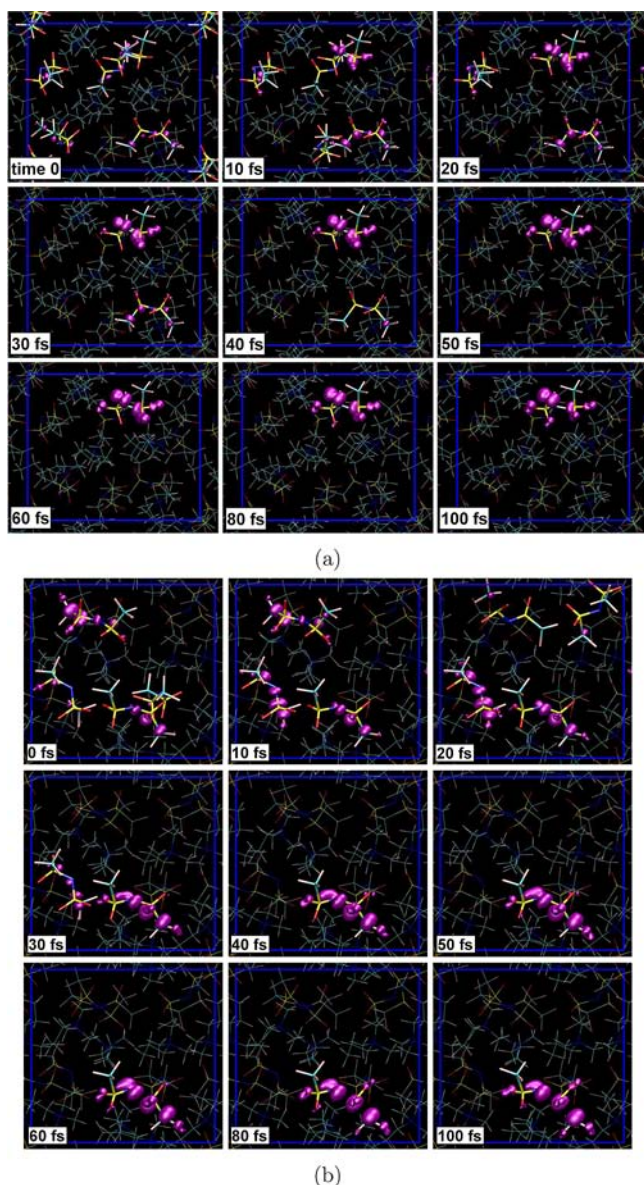


Figure 4. The time-dependent spin density ($\rho_\alpha - \rho_\beta$) for (a) [Pyrr_{1,4}][Tf₂N] and (b) [N₁₁₁₃][Tf₂N] ILs in the presence of an excess electron for snapshots between 0 and 100 fs showing the process of electronic localization. The isosurfaces were plotted at isovalue 0.005 l_e/bohr^3 for (a) and 0.05 l_e/bohr^3 for (b).

different delocalized adjacent parts of the liquid. Hence the separation of HOMO \uparrow and the LUMO \uparrow states (Figure 5a (left) and 5b (left)), the localization of the excess charge (Figure 4a and 4b), the disappearance of the broad band at very low transition energies (Figure 2a (left) and 2b (left)) and a set of structural changes in the anion over which the excess charge localizes (Figures S1 and S2) are all correlated. The electronic localization on a single anion marks the end of the dry electron state and the beginning of the trapped electron state. This localization process appears to be irreversible since further structural and chemical changes are associated with it (*vide infra*). Interestingly a similar phenomenon was recently reported albeit on a shorter 15–25 fs time scale in a study of excess electrons in water solvated DNA.⁵⁸

Just as the spin up channel plays the major role during the lifetime of the dry electron, the spin down channel will take

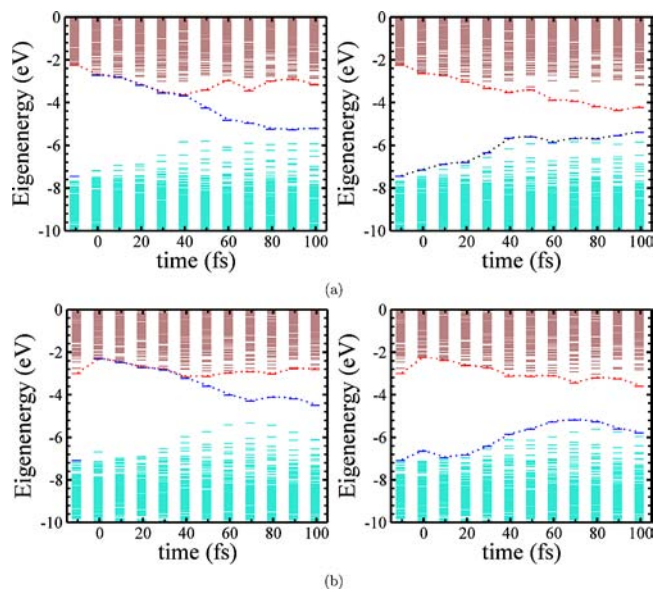


Figure 5. Energy diagram for (a) [Pyrr_{1,4}][Tf₂N] and (b) [N₁₁₁₃][Tf₂N] ILs in the presence of an excess electron during the first 100 fs. In both cases at negative time we show the band structure of the neat liquid without an excess electron. On the left panel, before 40 fs, blue and red dashes nearly overlap. On this sub-50 fs time scale HOMO \uparrow , LUMO \uparrow as well as other LUMOs have very similar energies.

center stage when we describe the trapped electron state. After addition of an excess electron in the spin up channel, the spin down channel also shows Stokes shift behavior. In this case the gap between HOMO \downarrow and LUMO \downarrow states diminishes and eventually transitions in the visible become possible between these states. This is reflected in the early spectrum of the spin down channel in Figure 2a (right) and 2b (right). We remind the readers that HOMO \downarrow corresponds to the highest occupied orbitals in the neat liquid without an excess electron and LUMO \downarrow is at the same level as HOMO \uparrow .

In brief, in these two systems, the dry electron corresponds to a very transient species in which the electron can delocalize over several anions and where low-energy near-IR transitions produce delocalization over other nearby anionic locations. The lifetime of the dry state is associated with the time it takes to find a suitable energy trap that results in spatial localization. Experimentally, this time will likely be longer than in our studies. This is because experiments produce electrons that have excess kinetic energy that needs to be dissipated.

3.2. The Nascent Trapped Electron State. Forty fs after the introduction of an excess electron in [N₁₁₁₃][Tf₂N] and [Pyrr_{1,4}][Tf₂N] several major events take place. The initially delocalized excess electron finds its way to a localized energy trap, and the almost degeneracy between HOMO \uparrow and LUMO \uparrow states breaks. This happens at the same time as structural reorganization occurs in the single anion on which the excess charge localizes.

Besides the Stokes shift observed in both spin channels (in one case HOMO \downarrow and LUMO \downarrow become closer in energy and in the other the liquid valence band comes close to HOMO \uparrow and LUMO \uparrow), other important changes also take place on a 300 fs time scale. Figure 5a and 5b shows that certain states in the neat liquid valence band separate from the rest and move up in energy closer to HOMO \uparrow or to LUMO \downarrow depending on the spin channel. These states are associated with the valence electrons of the particular anion in which the excess electron

localizes. However, as the gap between these states and HOMO \uparrow (or LUMO \downarrow) enters the visible range, this is only spectroscopically relevant to the spin down channel since both HOMO \uparrow -1 (in the liquid valence band) and HOMO \uparrow states are both occupied. Instead, spin down channel transitions from valence electrons of the doubly charged anion to LUMO \downarrow enter the visible range and have considerable oscillator strength (see Figure 2a (right) and 2b (right)). This is because these transitions are intra-ionic in nature, and therefore wave function overlap is high. At the same time as these transitions red shift, the broad band in the near-IR in the spin up channel due to the excess electron disappears as can be appreciated in Figure 2a (left) and 2b (left). The reasons for the disappearance of the broad low energy IR band are two-fold. First the excess electron transitions are interionic in nature (transferring the charge now localized in one anion to others) and therefore should have small wave function overlap, second the gap between HOMO \uparrow and states of higher energy widens and eventually moves out of the visible range making these transitions unavailable.

The nascent band from the spin down channel which initially appears in the visible and moves to the red (see Figure 2a (right) and Figure 2b (right)) is likely what ultrafast experiments probe. On a longer time scale than that accessible in our calculations, this band is experimentally seen as moving to the blue consistent with solvent reorganization. At least on the time scale we are able to study, this so-called “excess electron band” is of an odd nature since it does not really involve excitations of the excess electron! In fact these transitions are more “hole-like” than “electron-like”. This is because the nature of these transitions involve promoting an electron from a lower energy orbital in the doubly charged anion into LUMO \downarrow . In other words this process involves promoting holes down.

3.3. Picosecond Time Evolution of the Trapped Electron State. In the [Pyrr $_{1,4}$][Tf $_2$ N] and [N $_{1113}$][Tf $_2$ N] systems, the concept of a trapped electron has at least two meanings. The first one has to do with electronic localization. This process has a large driving force and is very fast on a 100 fs time scale. We expect our simulations to accurately capture this process. The second has to do with mechanical trapping or caging of the ion with the excess charge. This process is much more trajectory dependent and to accurately reproduce the average time-dependent spectra in ILs that are often structurally and dynamically heterogeneous a large ensemble of trajectories and perhaps larger simulation boxes may be required. To exemplify what is typical behavior in these [Tf $_2$ N $^-$] based systems we first show in Figure 6 that after initial charge localization, a single anion holds the extra charge for the whole duration of our simulations.

However, Figure S3 shows that the fluctuation of HOMO and LUMO energy levels in both spin channels is by no means over on a 50 fs time scale which is what it takes to initially localize the charge. In fact there are at least two more time scales that are relevant in the case of the trapped electron. The first one has to do with chemical reactivity and anionic dissociation at one of the N-S bonds resulting in two anionic fragments. The second one has to do with solvent reorganization and the escape of the fragments from their cage. Our studies are only able to address the initial portion of both these processes. At longer times inaccessible to the current work, the radical anion fragment (CF $_3$ SO $_2$ N $^-$) or subsequent degradation products, other electron acceptors or a nascent cavity, may be responsible for the experimentally observed

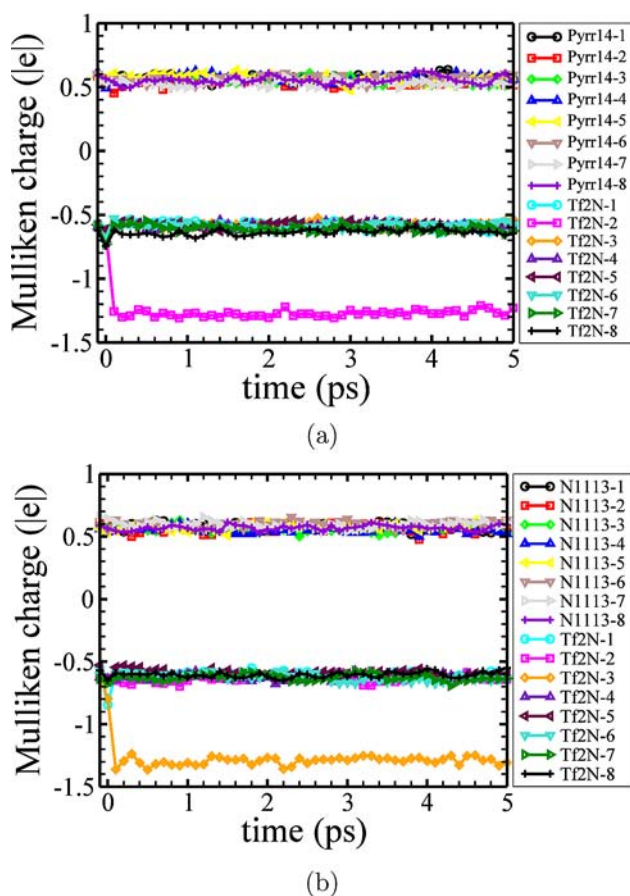


Figure 6. Mulliken charges for all individual ions in (a) [Pyrr $_{1,4}$]-[Tf $_2$ N] and (b) [N $_{1113}$][Tf $_2$ N] in the presence of an excess electron. Negative time corresponds to the neat liquids in the absence of the excess charge.

near-IR spectrum. It is also possible that inclusion of electron self-interaction corrections in the DFT calculations may favor yet a different mechanism with long time localization in a “complex type” of cavity-like state as described in refs 59 and 60. Two different mechanisms, a major one in which, as described in this article and supported by many experiments,^{26–32,61} [Tf $_2$ N $^-$] dissociates, and a secondary one involving electron cavity localization may account for the discrepancy between long time solvated electron radiolysis yields in water and alcohols $2\text{--}3 \times 10^{-7}$ mol J $^{-1}$ vs 0.7×10^{-7} mol J $^{-1}$ in ionic liquids.^{16,18}

Previous studies on imidazolium and pyridinium systems coupled with the chloride anion show the possibility of alternating localization and delocalization of the excess charge.^{39,40} This does not take place in the current studies perhaps because of the break in symmetry caused by the dissociation of [Tf $_2$ N $^-$]. The two trajectories we describe in this work show initial cleavage at one of the N-S bonds of the doubly charged anion, but indications exist that the S-C bond is labile and will also break. Figure 7 shows for both systems the bond distance between the dissociating N-S atoms as well as the abnormal S-C vibrations of large amplitude in the separating fragments. Figure S4 shows that at about 5 ps the individual Mulliken charge of each of the two dissociating fragments converges to a similar value between -0.6 and -0.7 |e|, analogous to that of typical singly charged anions in the liquid. The dissociation pathway observed in our current *ab*

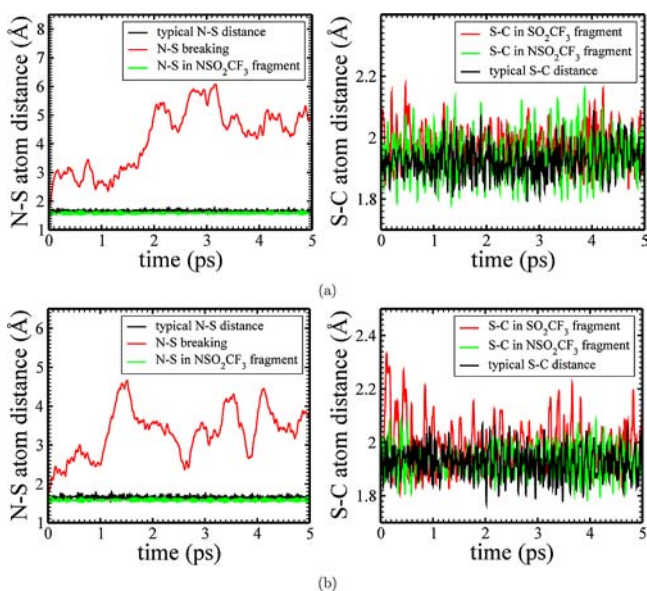


Figure 7. N–S and S–C bond lengths for the breaking anion with the excess charge in the case of (a) [Pyr_{1,4}][Tf₂N] and (b) [N₁₁₁₃][Tf₂N].

initio dynamics was already predicted from minimizations in the liquid and gas phases in our previous study.⁴¹ The MacFarlane

group had also speculated on the effect of an excess charge on a single [Tf₂N[−]] anion in the gas phase.⁶² They noticed that the S–N–S bonds in the LUMO of the [Tf₂N[−]] anion are of π^* antibonding nature and speculated that an excess electron in this orbital would lead to initial S–N bond breaking.

Figure 8a and 8b combines a time snapshot of the spectrum as well as isosurfaces of HOMO \downarrow and LUMO \downarrow wave functions which give rise to one of the main relevant transitions in the lower energy band. The reader is reminded that these are “hole-like” transitions in that a spin down channel electron is promoted leaving a hole that moves down in the liquid valence band. In our trajectories the broad absorption band experimentally associated with the excess electron appears, disappears and moves in frequency as the dissociating fragments move in their solvent cage and recombine in different orientations. These significant changes in the time-dependent spectrum have to do with distance and relative orientation of the breaking fragments as well as the overlap and relative symmetry of HOMO \downarrow and LUMO \downarrow wave functions as well as other energy relevant states. As opposed to the early femtosecond spectral changes, the later form of the spectrum is very trajectory dependent. A large ensemble of such trajectories is needed in order to reproduce the time-dependent experimental picosecond signal.

Interestingly, as fragments remain caged, relevant optical transitions often involve electron transfer from one fragment to

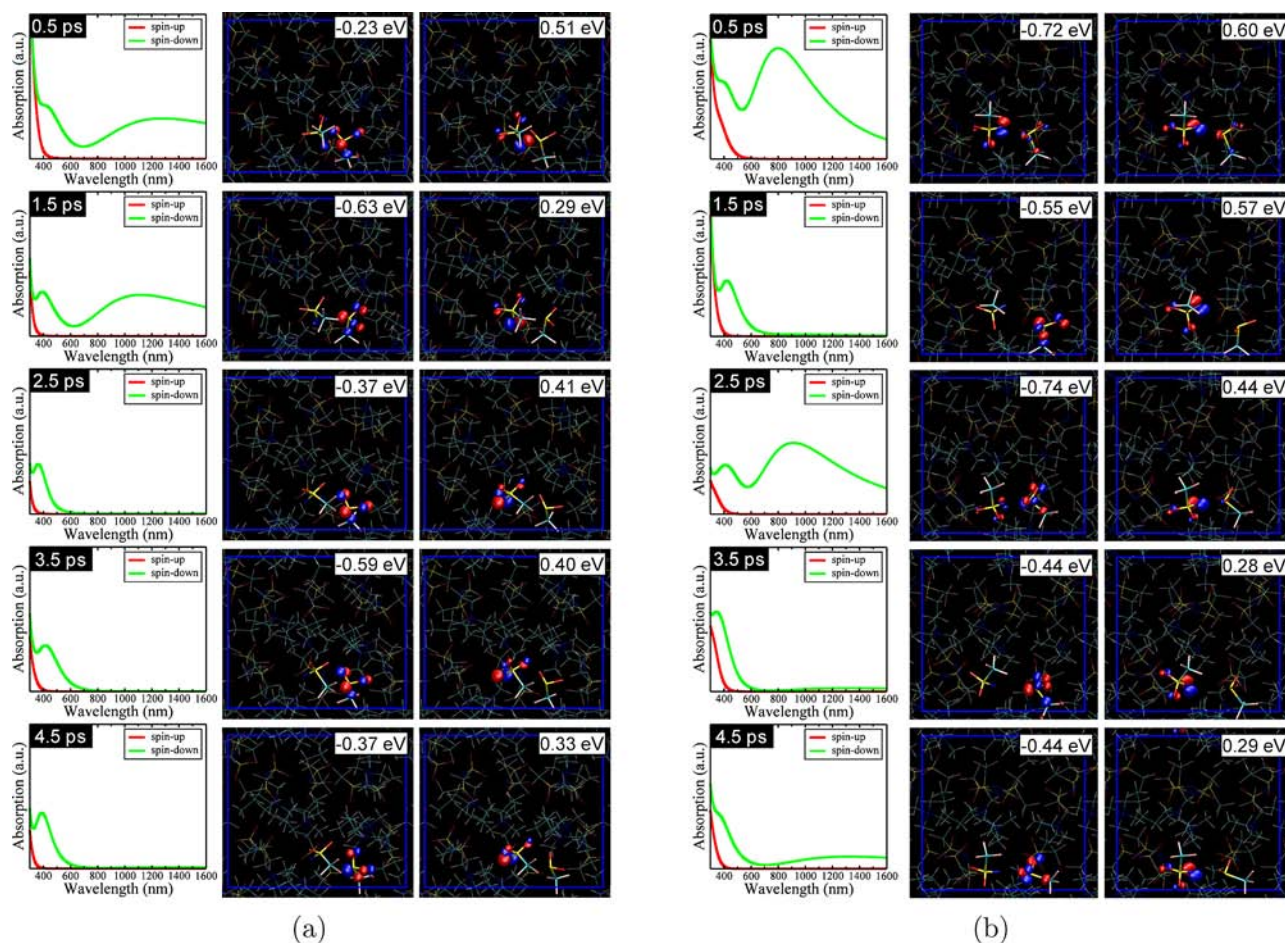


Figure 8. Time-dependent spectra for both spin channels and the HOMO \downarrow to LUMO \downarrow wave functions in the case of (a) [Pyr_{1,4}][Tf₂N] and (b) [N₁₁₁₃][Tf₂N] in the presence of an excess electron. The wave functions are plotted using the same isovalue. For each wave function we include its energy eigenvalue. In all cases, for clarity, the value of the Fermi energy has been shifted to zero.

the other following the rules of intermolecular electron transfer. We know this because HOMO \downarrow and LUMO \downarrow transitions involve promotion of an electron localized in one of the dissociating fragments to a state mostly localized on the other fragment. This can be seen in some of the snapshots depicted in Figure 8 as well as by analysis of wave function coefficients. This type of electron transfer becomes less efficient when symmetry is not appropriate or when fragments rotate and the N–S distance increases significantly. In fact in the case of the [Pyrr_{1,4}][Tf₂N] we see the signal disappear during several picoseconds. This occurs because an almost 180° rotation of one of the fragments with respect to the other results in an N–S distance of about 6 Å, see Figure 7a (left).

4. CONCLUSIONS

This article identifies the chemical nature of the elusive “dry” and “trapped” electron states in the [Pyrr_{1,4}][Tf₂N] and [N₁₁₁₃][Tf₂N] systems and makes a set of spectroscopic predictions that can be experimentally corroborated once short femtosecond experiments become available. On a 50 fs time scale an excess electronic charge goes from delocalized over several [Tf₂N⁻] anions to localized on a single one. This localization process is associated with the disappearance of a broad low-energy band in the spin up channel (which in our simulations holds the excess electron). This very early band corresponds to transitions that displace the dry electron from one group of anions to adjacent anionic locations with high overlap. Early time evolution results in localization of the excess charge on a single anion. At this point HOMO \uparrow and nearby LUMO \uparrow energies begin to separate as the nascent trapped electron state forms and the doubly charged anion begins to dissociate. The trapped state is characterized by a localized electron on a single [Tf₂N⁻] anion for which transitions of the excess electron are no longer possible, but instead transitions in the opposite spin channel become available. These transitions that on a several hundred femtosecond time scale move to the red promote electrons of the doubly charged anion leaving a hole behind.

On a picosecond time scale the doubly charged anion dissociates by breaking one of the N–S bonds. At this point, HOMO \downarrow to LUMO \downarrow transitions are often dominated by electron transfer from one fragment to the other. The spectrum significantly changes as fragments bounce and rotate in their solvent cage. Both the frequency of the transitions as well as amplitude fluctuate with the distance and orientation of the fragments and in cases the band disappears as fragments drift apart or take on different relative orientations.

■ ASSOCIATED CONTENT

Supporting Information

Early S–N bond distances, S–N–S angles, energy diagrams, and the time history of Mulliken charges for the dissociating fragments. This information is available free of charge via the Internet at <http://pubs.acs.org/>

■ AUTHOR INFORMATION

Corresponding Author

claudio-margulis@uiowa.edu

Notes

The authors declare no competing financial interest.

■ ACKNOWLEDGMENTS

This work was supported by the U.S. Department of Energy, Office of Basic Energy Sciences, Division of Chemical Sciences, Geosciences, and Biosciences under contract DE-SC0008644 awarded to C.J.M. C.J.M. would like to thank Dr. James Wishart and Prof. David Blank for instructive discussions.

■ REFERENCES

- (1) Castner, E. W., Jr.; Margulis, C. J.; Maroncelli, M.; Wishart, J. F. *Annu. Rev. Phys. Chem.* **2011**, *62*, 85–105.
- (2) Castner, E. W., Jr.; Wishart, J. F. *J. Chem. Phys.* **2010**, *132*, 120901.
- (3) MacFarlane, D. R.; Seddon, K. R. *Aust. J. Chem.* **2007**, *60*, 3–5.
- (4) Ohno, E., H. *Electrochemical Aspects of Ionic Liquids*, 2nd ed.; John Wiley & Sons: Hoboken, NJ, 2011.
- (5) Wishart, J. F. *Energy Environ. Sci.* **2009**, *2*, 956–961.
- (6) Plechkova, N. V.; Seddon, K. R. *Chem. Soc. Rev.* **2008**, *37*, 123–150.
- (7) Hough, W. L.; Rogers, R. D. *Bull. Chem. Soc. Jpn.* **2007**, *80*, 2262–2269.
- (8) Weingärtner, H. *Angew. Chem., Int. Ed.* **2008**, *47*, 654–670.
- (9) Allen, D.; et al. *Green Chem.* **2002**, *4*, 152–158.
- (10) Wishart, J. F.; Shkrob, I. A. In *Ionic Liquids: From Knowledge to Application*; Plechkova, N. V., Rogers, R. D., Seddon, K., Eds.; ACS: Washington, D.C., 2009; Vol. 1030; pp 119–134.
- (11) Shkrob, I. A.; Wishart, J. F. *J. Phys. Chem. B* **2009**, *113*, 5582–5592.
- (12) Wishart, J. J. *Phys. Chem. Lett.* **2010**, *1*, 1629–1630.
- (13) Funston, A. M.; Wishart, J. F. In *Ionic Liquids IIIA: Fundamentals, Progress, Challenges, and Opportunities, Properties and Structure*; Rogers, R. D., Seddon, K. R., Eds.; ACS: Washington, D.C., 2005; Vol. 901; pp 102–116.
- (14) Grodkowski, J.; Neta, P.; Wishart, J. F. *J. Phys. Chem. A* **2003**, *107*, 9794–9799.
- (15) Wishart, J. F. *J. Phys. Chem. Lett.* **2010**, *1*, 3225–3231.
- (16) Wishart, J. F. In *Ionic Liquids as Green Solvents: Progress and Prospects*; Rogers, R. D., Seddon, K. R., Eds.; ACS: Washington, D.C.; 2003; Vol. 856; pp 381–396.
- (17) Wishart, J. F.; Funston, A. M.; Szreder, T.; Cook, A. R.; Gohdo, M. *Faraday Discuss.* **2012**, *154*, 353–363.
- (18) Wishart, J. F.; Neta, P. *J. Phys. Chem. B* **2003**, *107*, 7261–7267.
- (19) Behar, D.; Gonzalez, C.; Neta, P. *J. Phys. Chem. A* **2001**, *105*, 7607–7614.
- (20) Behar, D.; Neta, P.; Schultheisz, C. *J. Phys. Chem. A* **2002**, *106*, 3139–3147.
- (21) Yang, J.; Kondoh, T.; Norizawa, K.; Nagaishi, R.; Taguchi, M.; Takahashi, K.; Katoh, R.; Anishchik, S. V.; Yoshida, Y.; Tagawa, S. *Radiat. Phys. Chem.* **2008**, *77*, 1233–1238.
- (22) Takahashi, K.; Sato, T.; Katsumura, Y.; Yang, J.; Kondoh, T.; Yoshida, Y.; Katoh, R. *Radiat. Phys. Chem.* **2008**, *77*, 1239–1243.
- (23) Asano, A.; Yang, J. F.; Kondoh, T.; Norizawa, K.; Nagaishi, R.; Takahashi, K.; Yoshida, Y. *Radiat. Phys. Chem.* **2008**, *77*, 1244–1247.
- (24) Kondoh, T.; Asano, A.; Yang, J. F.; Norizawa, K.; Takahashi, K.; Taguchi, M.; Nagaishi, R.; Katoh, R.; Yoshida, Y. *Radiat. Phys. Chem.* **2009**, *78*, 1157–1160.
- (25) Grodkowski, J.; Neta, P. *J. Phys. Chem. A* **2002**, *106*, 5468–5473.
- (26) Berthon, L.; Nikitenko, S.; Bisel, I.; Berthon, C.; Faucon, M.; Saucerotte, B.; Zorz, N.; Moisy, P. *Dalton Trans.* **2006**, 2526–2534.
- (27) Bosse, E.; Berthon, L.; Zorz, N.; Monget, J.; Berthon, C.; Bisel, I.; Legand, S.; Moisy, P. *Dalton Trans.* **2008**, 924–931.
- (28) Le Rouzo, G.; Lamouroux, C.; Dauvois, V.; Dannoux, A.; Legand, S.; Durand, D.; Moisy, P.; Moutiers, G. *Dalton Trans.* **2009**, 6175–6184.
- (29) Shkrob, I. A.; Chemerisov, S. D.; Wishart, J. F. *J. Phys. Chem. B* **2007**, *111*, 11786–11793.

- (30) Shkrob, I. A.; Marin, T. W.; Bell, J. R.; Luo, H.; Dai, S.; Hatcher, J. L.; Rimmer, R. D.; Wishart, J. F. *J. Phys. Chem. B* **2012**, *116*, 2234–2243.
- (31) Shkrob, I. A.; Marin, T. W.; Chemerisov, S. D.; Hatcher, J. L.; Wishart, J. F. *J. Phys. Chem. B* **2011**, *115*, 3889–3902.
- (32) Shkrob, I. A.; Marin, T. W.; Chemerisov, S. D.; Wishart, J. F. *J. Phys. Chem. B* **2011**, *115*, 3872–3888.
- (33) Takahashi, K.; Suda, K.; Seto, T.; Katsumura, Y.; Katoh, R.; Crowell, R. A.; Wishart, J. F. *Radiat. Phys. Chem.* **2009**, *78*, 1129–1132.
- (34) Katoh, R.; Yoshida, Y.; Katsumura, Y.; Takahashi, K. *J. Phys. Chem. B* **2007**, *111*, 4770–4774.
- (35) Molins i Domenech, F.; FitzPatrick, B.; Healy, A. T.; Blank, D. A. *J. Chem. Phys.* **2012**, *137*, 034512.
- (36) Chandrasekhar, N.; Schalk, O.; Unterreiner, A. N. *J. Phys. Chem. B* **2008**, *112*, 15718–15724.
- (37) Nese, C.; Unterreiner, A.-N. *Phys. Chem. Chem. Phys.* **2010**, *12*, 1698–1708.
- (38) Chandler, D.; Leung, K. *Annu. Rev. Phys. Chem.* **1994**, *45*, 557–591.
- (39) Wang, Z. P.; Zhang, L.; Chen, X. H.; Cukier, R. I.; Bu, Y. X. *J. Phys. Chem. B* **2009**, *113*, 8222–8226.
- (40) Wang, Z. P.; Zhang, L.; Cukier, R. I.; Bu, Y. X. *Phys. Chem. Chem. Phys.* **2010**, *12*, 1854–1861.
- (41) Margulis, C. J.; Annapureddy, H. V.; De Biase, P. M.; Coker, D.; Kohanoff, J.; Del Pópolo, M. G. *J. Am. Chem. Soc.* **2011**, *133*, 20186–20193.
- (42) Muller, E. A.; Strader, M. L.; Johns, J. E.; Yang, A.; Caplins, B. W.; Shearer, A. J.; Suich, D. E.; Harris, C. B. *J. Am. Chem. Soc.* **2013**, *135*, 10646–10653.
- (43) Canongia Lopes, J. N.; Pádua, A. A. H. *J. Phys. Chem. B* **2004**, *108*, 16893–16898.
- (44) Canongia Lopes, J. N.; Pádua, A. A. H. *J. Phys. Chem. B* **2006**, *110*, 19586–19592.
- (45) Price, M. L. P.; Ostrovsky, D.; Jorgensen, W. L. *J. Comput. Chem.* **2001**, *22*, 1340–1352.
- (46) Kashyap, H. K.; Santos, C. S.; Murthy, N. S.; Hettige, J. J.; Kerr, K.; Ramati, S.; Gwon, J.; Gohdo, M.; Lall-Ramnarine, S. I.; Wishart, J. F.; Margulis, C. J.; Castner Jr., E. W. *J. Phys. Chem. B* **2013**, published as ASAP doi: 10.1021/jp403518j.
- (47) Artacho, E.; Anglada, E.; Diéguez, O.; Gale, J. D.; Garca, A.; Junquera, J.; Martin, R.; Ordejón, P.; Pruneda, J.; Sánchez-Portal, D.; Soler, J. M. *J. Phys.: Condens. Matter* **2008**, *20*, 064208.
- (48) Soler, J. M.; Artacho, E.; Gale, J. D.; García, A.; Junquera, J.; Ordejón, P.; Sánchez-Portal, D. *J. Phys.: Condens. Matter* **2002**, *14*, 2745–2779.
- (49) Sánchez-Portal, D.; Ordejón, P.; Artacho, E.; Soler, J. M. *Int. J. Quantum Chem.* **1997**, *65*, 453–461.
- (50) Troullier, N.; Martins, J. L. *Phys. Rev. B* **1991**, *43*, 1993–2006.
- (51) Perdew, J. P.; Burke, K.; Ernzerhof, M. *Phys. Rev. Lett.* **1996**, *77*, 3865–3868.
- (52) Hunt, P.; Sprik, M.; Vuilleumier, R. *Chem. Phys. Lett.* **2003**, *376*, 68–74.
- (53) Hunt, P.; Sprik, M. *ChemPhysChem* **2005**, *6*, 1805–1808.
- (54) Neumann, S.; Eisfeld, W.; Sobolewski, A. L.; Domcke, W. *J. Phys. Chem. A* **2006**, *110*, 5613–5619.
- (55) Hübsch, A.; Endres, R. G.; Cox, D. L.; Singh, R. R. *Phys. Rev. Lett.* **2005**, *94*, 178102.
- (56) Machón, M.; Reich, S.; Thomsen, C.; Sánchez-Portal, D.; Ordejón, P. *Phys. Rev. B* **2002**, *66*, 155410.
- (57) Ong, S. P.; Andreussi, O.; Wu, Y.; Marzari, N.; Ceder, G. *Chem. Mater.* **2011**, *23*, 2979–2986.
- (58) Smyth, M.; Kohanoff, J. *Phys. Rev. Lett.* **2011**, *106*, 238108.
- (59) Uhlig, F.; Marsalek, O.; Jungwirth, P. *J. Phys. Chem. Lett.* **2012**, *3*, 3071–3075.
- (60) Uhlig, F.; Marsalek, O.; Jungwirth, P. *J. Phys. Chem. Lett.* **2013**, *4*, 338–343.
- (61) Yuan, L.; Xu, C.; Peng, J.; Xu, L.; Zhai, M.; Li, J.; Wei, G.; Shen, X. *Dalton Trans.* **2009**, 7873–7875.
- (62) Howlett, P. C.; Izgorodina, E. I.; Forsyth, M.; MacFarlane, D. R. *Z. Phys. Chem.* **2006**, *220*, 1483–1498.